

Research Journal of Pharmaceutical, Biological and Chemical Sciences

Synthesis and Characterization of Graphene Oxide/ Crosslinked Chitosan Nanaocomposite for Lead Removal Form Aqueous Solution.

M A Moharram¹, K MT Ereiba², Walid El hotaby¹, and AM Bakr^{1*}.

¹Spectroscopic Department, Physics Division, National Research Center Cairo, Egypt.

²Physics Department, Faculty of Science, El Azhar University, Cairo, Egypt.

ABSTRACT

In this work, graphene oxide (GO) was firstly prepared using a modified Hummers method from natural graphite powder. Samples of graphene oxide crosslinked chitosan nanocomposites with different molar ratios of graphene oxide (GOCH) were prepared. The morphology, crystalline structure and molecular structure of the prepared nanocomposites were investigated using different analytical methods. SEM micrographs revealed that the addition of GO to chitosan increases folding and roughness of the composites surfaces which in turn leads to an increase in the surface area. The FTIR spectrum of GO proved that there is a chemical interaction between GO and the chitosan chains take place via hydrogen bonding. The batch experiments were carried out for adsorption of Pb⁺² onto the prepared nanocomposites. The adsorption results showed that the optimum pH value was 5. While the optimum initial dose of adsorbent material was 0.2 gram. It was concluded that the addition of GO can obviously enhances the adsorption features of chitosan. Also, the adsorption kinetics of the nanocomposites were discussed.

Key words: Graphene oxide, Chitosan, Crosslinking, Beads, Adsorption kinetics.

**Corresponding author*

INTRODUCTION

Because of the toxic effect to the human beings and other animals and plants in the environment, contamination with heavy metal of various water resources is of great concern. Although heavy metals are natural components of the Earth's crust, their concentrations in an aquatic environments have increased due to mining and industrial activities and geochemical processes. Heavy metals are common in industrial applications such as the manufacture of pesticides, batteries, mining operations, alloys, metal plating facilities, textile dyes, tanneries, etc [1].

Different treatment techniques for wastewater laden with heavy metals have been developed in recent years to decrease the amount of wastewater produced and to improve the quality of the treated effluent. Although various treatments such as chemical precipitation, coagulation–flocculation, reverse osmosis, ultra-filtration, electro-dialysis flotation and ion exchange can be employed to remove heavy metals from contaminated wastewater, they have their inherent advantages and limitations in application [2-11]. Among all of the methods, the adsorption seems to be a more suitable method for the adsorption of heavy metals due to low cost, simply operating, no or little use of organic solvents, and high efficiency [12-15].

Ideal graphene is a 2D crystal composed of monolayers of carbon atoms arranged in a honeycombed network with six-membered rings. Graphene has become a sparkling rising star on the horizon of materials science due to its extraordinary electrical, thermal, and mechanical properties. Graphene oxide (GO) has gained an explosion of interest and opened up a new research area for material science. Recent researches have indicated that GO proved to be a promising material to adsorb metal ions due to their extraordinary mechanical strength and relatively large specific area [16-18].

Chitosan, the linear cationic aminopolysaccharide, among biosorbents is the most abundant biopolymer in nature after cellulose. Owing to the outstanding properties of chitosan, such as nontoxic, biocompatibility, hydrophilic, antibacterial activity, it has been extensively used in various fields, such as biomaterials, textile, drug delivery, environmental protection, and metallurgy [19-22].

Chitosan, composed mainly of poly(b-1-4)-2-amino-2-deoxy- D-glucopyranose, is obtained from deacetylation process of chitin. The amine and two hydroxyl groups on each glucosamine monomer act as adsorption sites, especially the amine groups which are strongly reactive with metal ions. Therefore, chitosan has high adsorption capacity but due to its low porosity, weak mechanical property and easily soluble in slightly acidic medium; its fullest capacities are not met. Many modifications such as physical and chemical modifications can be carried out to chitosan in order to increase its adsorption capacity. Physical and chemical modifications can prevent dissolution of chitosan in acidic medium and improve the mechanical strength. One of the most spread chemical modifications is crosslinking process, grafting of a new functional group and acetylation [23-25].

Based on favorable adsorption properties of graphene oxide (GO), and inherent properties of chitosan some researchers have explored the possibility of graphene oxide / chitosan composite as biosorbents [26-31].

Therefore, in our laboratory, effort has been made to fabricate adsorptive graphene oxide crosslinked chitosan beads and investigate its molecular structural. Also the factors controls the efficiency of the prepared nanocomposites will be studied; these factors included the molar ratios between GO and chitosan, initial pH value of the adsorbate solution, initial adsorbent dose and contact time. In addition the adsorption kinetics will be study in order to found the suitable kinetic model able to describe the adsorption process.

EXPERIMENTAL

Materials

Graphite powder with a size less than 20 μ m was purchased from Sigma-Aldrich. Chitosan (low molecular weight 150000) and hydrogen peroxide were bought from ROTH, Germany. Sodium tripolyphosphate ($\text{Na}_5\text{O}_{10}\text{P}_3$) were purchased from Sigma-Aldrich, USA. Sulphuric acid (98%) was obtained from Fisher. Sodium nitrate (99%) was purchased from ACROS, Belgium. All the reagents were of analytical grade or highest purity available, and used without further purification. Doubly distilled water was used throughout the experiments.

Synthesis of graphene oxide (GO)

Purified graphite was used to prepare GO according to the well-known Hummer's method with some modification [32]. Firstly, 5.0 g of graphite powder and 115 mL 98% H₂SO₄ were put into a 5 L flask. The mixture was kept at an ice-water bath in order to keep the temperature around 0°C with continuous stirring until the graphite full dissolved. Then 2.5 g of NaNO₃ was added, after 10 min 15 g of KMnO₄ was added by batch addition while stirring. Then the flask was kept at 35°C for 3 h. After 3h, 230 ml of distilled water was slowly added, and the temperature of the mixture was kept at 98 °C for 20 min. Then, the reaction was stopped by adding distilled water (700 mL) and H₂O₂ (50 mL, 30 %) The solution's color transformed to brilliant yellow. The obtained powder was washed, filtered, and dried at 60 °C for 24 h.

Preparation of graphene oxide crosslinked chitosan beads (GOCH)

Certain amount of the prepared GO powder was dispersed into 200 ml 1% (v/v) acetic acid solution and treated by ultrasound for 15 min at room temperature. 4.0 g of chitosan powder was added into the suspension under stirring until it was completely dissolved and mix with GO uniformly.

After rested for 1 h, the well-distributed suspension was dropped into 0.05 M of TPP aqueous solution using a 0.8 mm diameter injector and the injection rate was about 150 ml/h the beads were formed immediately in the TPP solution and kept overnight to solidified then collect the prepared beads and washed several times by ultrapure water until the pH value of the water was nearly neutral. Finally, the beads were isolated by filtration and were left to air-dry in Petri dish for two days then collected and saved in closed vile.

A series of graphene oxide / chitosan composites beads coded as H5, H10, H15, and H20 were prepared by varied the weight of GO into the composite as 5 wt%, 10 wt%, 15wt % and 20 wt% respectively. In addition, cross-linked chitosan, coded as H0, was also prepared according to the same method without adding GO.

Batch experiments

In the pH studies, 0.05 g of the prepared beads and 100mL lead solution (20 ppm) with a range of pH values from 3.0 to 6.0, which was adjusted with 0.1M HCl or 0.1M NaOH solution, Adsorbent dosage experiments were conducted by shaking 100 mL Pb²⁺ solutions (20 ppm) with different masses of the prepared beads (0.05- 0.2 g) at room temperature for 2 h. In kinetic experiments and to study the effects of contact time, 0.2 g of the adsorbent was added to a 100 mL solution of Pb²⁺ (20 ppm) and shaken at room temperature. Samples of 1 mL were taken at predetermined time intervals for the analysis of the lead ions in the solution. All the batch experiments were performed in pent replicate and the average data were used in data analysis.

The adsorption capacity of the adsorbent beads was calculated using equation (1):

$$Q_t = \frac{(C_o - C_e) * V}{W} \quad (1)$$

Where C_o is the initial concentration of Cd (II) (mg/L), C_e is the final concentration of Cd (II) (mg/L), V is the volume of the heavy metal ions solution (L) and W is the weight of dry beads (g). The percentage of removal for Pb (II) was calculated using equation (2):

$$\% \text{ removal of Pb} = \frac{C_i - C_o}{C_i} \times 100 \quad (2)$$

Characterizations

Jasco FT/IR-430 Fourier Transform Infrared Spectrometer was used for recording the IR spectra. Spectra were recorded in a spectral range of 4000–400 cm⁻¹, resolution 2 cm⁻¹ and scan speed 2mm/sec. The structure of GO nanocomposites were investigated by Broker D8 Advance, Germany X-ray diffraction (XRD) with CuK α 40kV/40mA and an incidence angle of 0.5° with wavelength equal to 1.5418 Å. The diffraction

patterns were recorded automatically with a scanning rate of $2\theta=2$ (deg/min). The samples were observed using a ((JEM-1230FX, JEOL Co., Tokyo, Japan) operated at 120 kV. High magnification (20Kx, 150Kx) bright field (BF) images and selected area diffraction (SAD) patterns were recorded) transmission electron microscope. SEM characterization was carried out using a Quanta FEG 250 type instruments in vacuum environment. The solutions obtained in the adsorption process were analyzed using flame AAS. The instrument applied was a Thermo Elemental SOLAAR M6 Series atomic absorption spectrometer. Element content of aqueous solutions was determined with hollow cathode lamps.

RESULTS AND DISCUSSION

Morphological structure of graphene oxide crosslinked chitosan nanocomposites (GOCH)

The morphological structure of GO nanosheets was investigated through HR-SEM and HR-TEM observations. Figure 1 displays that raw graphite consists of randomly aggregated, thin, crumpled sheets closely associated with each other, while, GO nanosheet as it shown in figure 2, appears flat and transparent with some wrinkles and folding on the surface, which may be attributed to deformation upon the exfoliation and restacking processes of graphite.

Independent GO nanosheets were observed through HR-TEM micrographs (fig 3). The individual nanosheets have sizes extending from tens to several hundreds of square nanometers.

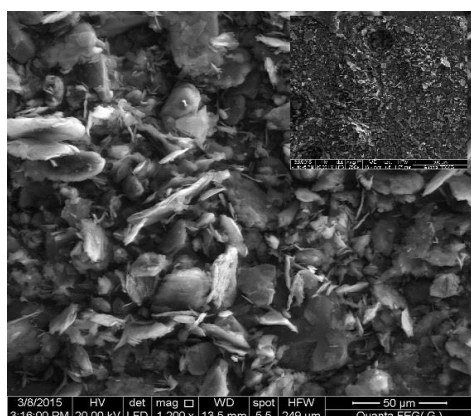


Figure 1: HR-SEM micrograph of graphite powder

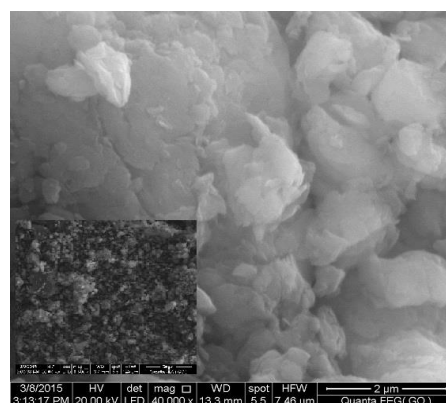


Figure 2: HR-SEM micrograph of GO powder

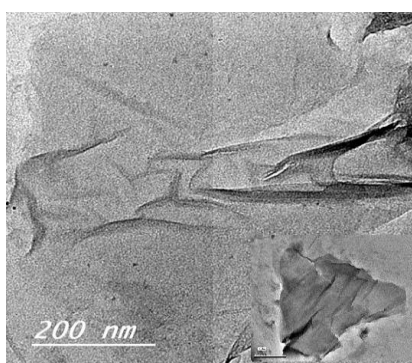


Figure 3: TEM micrograph of GO

SEM micrograph of crosslinked chitosan, sample H0, reveals that the surface of the sample is very smooth and shows no cracks as it is shown in figure (4). Careful investigation of TEM figure (9) reveals that the cross linked chitosan has average particle size about 50 nm. It could be concluded that the process of crosslinking reduced the particle size of chitosan to nano-scale particle size.

Figures 5-8 represent the HR-SEM micrographs for GOCH samples H5, H10, H15 and H20 respectively. The presence of GO in crosslinked chitosan composite obviously changed the surface morphology by a great deal. There are dramatically increasing in the roughness as well as a clear large folding and deep groves as the GO increases. The HR-TEM micrographs of GOCH samples H10 and H20 are shown in figures 10 and 11 respectively. The images show that GO well exfoliated within chitosan matrix with nanoscale size.

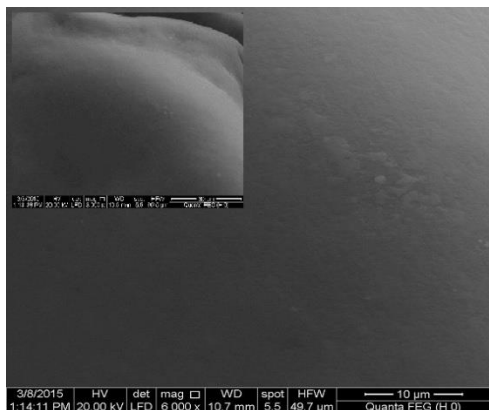


Figure 4: SEM micrograph of crosslinked chitosan(H0)

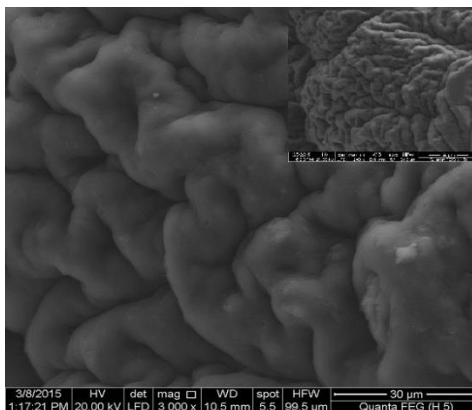


Figure 5: SEM micrograph of GO chitosan composite (H5)

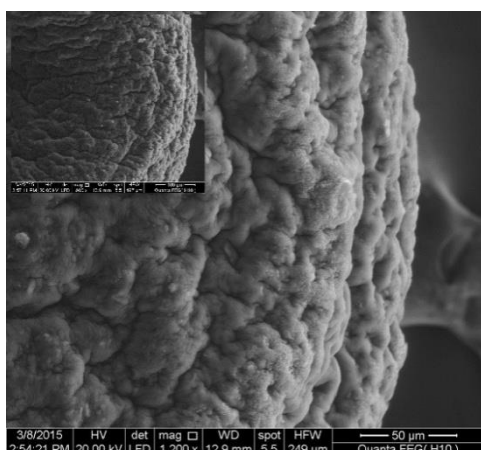


Figure 6: SEM micrograph of GO chitosan composite (H10)

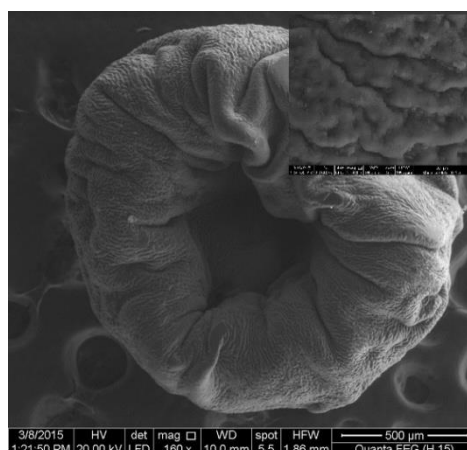


Figure 7: SEM micrograph of GO chitosan composite (H15)

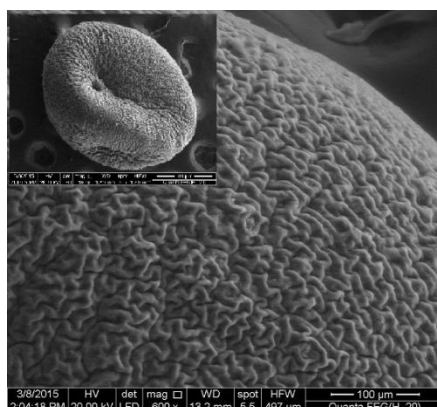


Figure 8: SEM micrograph of GO chitosan composite (H20)

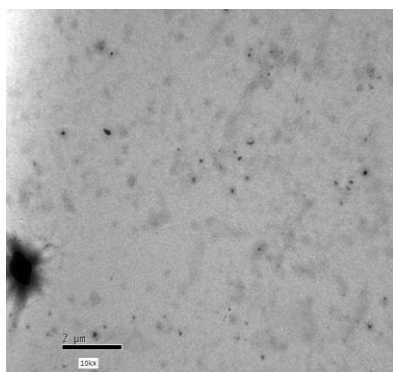


Figure 9: TEM micrograph of crosslinked chitosan(H0)

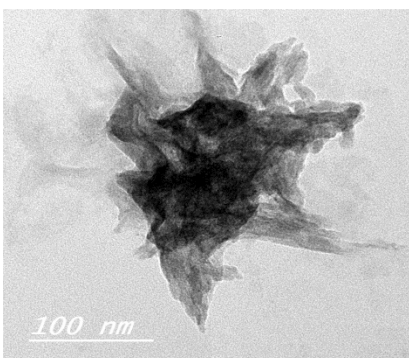


Figure 10: TEM micrograph of GO chitosan composite (H10)

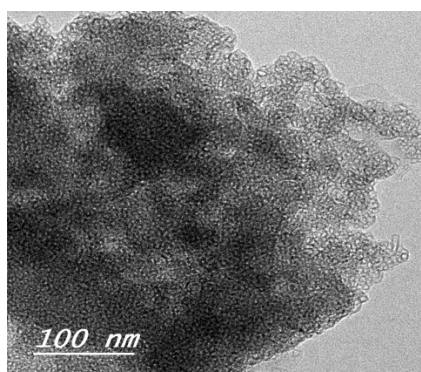


Figure 11: TEM micrograph of GO chitosan composite (H20)

Infrared spectrum of GOCH

Figure 12 displays the FTIR spectra of GO, Chitosan Powder (CH) and GOCH. The FTIR spectrum of GO shows a high broad band at 3400 cm^{-1} related to the stretching vibration of the hydroxyl group O–H. The absorption band at 1710 cm^{-1} was ascribed to C=O while the peak found at 1620 cm^{-1} can be assigned to the C–C stretching and absorbed hydroxyl groups in the GO. The small absorption band at 1520 cm^{-1} is related to the vibration of C–C stretching vibration in graphitic domains found in S^{-1} . C–OH (1392 cm^{-1}) and C–O–C (1036 cm^{-1}) are also clearly observed. These main characteristic peaks of GO are similar to those reported in the literature [33-35]. The FTIR spectrum of GO reveals the presence of the oxygen-containing functional groups, which include bands at 3400 cm^{-1} (stretching vibration of the hydroxyl group O–H) 1036 cm^{-1} (C–O stretching vibration of epoxide) and 1710 cm^{-1} (C=O stretching of carbonyl and carboxyl groups at edge s of the GO networks).

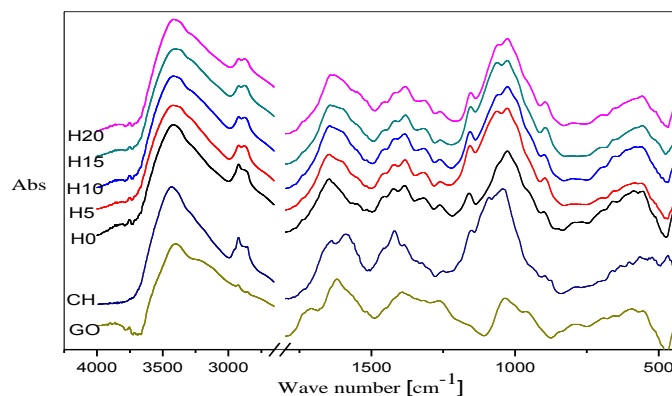


Figure 12: FT-IR spectra of GO, Chitosan Powder (CH) and GOCH.

The infrared spectrum of chitosan powder is shown in figure (12). Careful examination of chitosan spectrum reveals that the major peak located at 3440 cm^{-1} is due to the overlapping of O–H and N–H stretching vibrations bands, the peak at 2921 cm^{-1} is assigned to aliphatic C–H stretching vibrations, the peaks at 1650 and 1590 cm^{-1} are attributed to the secondary amide C=O bond of the remaining acetamido groups (Amide I) and the –NH bending vibration of NH_2 groups (Amide II), respectively. The peak at 1420 cm^{-1} can be assigned to C–H bending vibration, while the peaks at 1255 and 1152 cm^{-1} are due to the C–N stretching vibrations. The remaining peaks at 1093 and 1043 cm^{-1} are attributed to the C–O stretching vibrations in C–OH. These assignments are in good agreement with those reported in the literature [36-37]

Figure (12) displays the major absorption peaks of the ordinary spectrum of cross linked chitosan appear at 3432 cm^{-1} which is attributed to overlapping of O–H and N–H stretching vibrations.

The band at about 1640 cm^{-1} is attributed to P=O of the –POH groups found in the tripolyphosphate molecule. NH_3^+ in C-TPP beads is expressed by the peak at 1549 cm^{-1} . Besides the characteristic peaks of chitosan powder the crosslinked chitosan spectrum exhibits a new peak at 1253 cm^{-1} which is assigned as P=O stretching. The peak at 1324 cm^{-1} is a characteristic peak for the N- acetyl glucosamine while the peak at 888 cm^{-1} corresponds to the characteristic absorption of β -d-glucose unit. These results are in good agreement with the assignments reported in the literature [26].

The previous discussion confirmed that the crosslinking of chitosan produces the following changes in the spectral features of chitosan. The presence of a new peak at 1253 cm^{-1} indicates the presence of P=O molecules. The peak at 1590 cm^{-1} corresponding to N–H vibration in chitosan spectrum shifted to 1549 cm^{-1} . The last frequency is attributed to NH_3^+ . This peak supports the idea that crosslinking process is formed by attaching two chitosan molecules to each other through NH_3^+ group and through TPP molecule as is shown in figure (12). It is clear from the spectrum of chitosan powder that all peaks related to N- atoms are affected by crosslinking process which supports the previous mentioned idea.

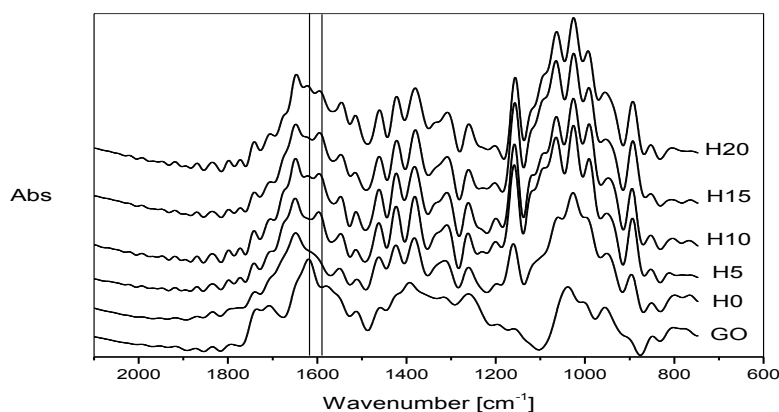


Figure 13: Deconvoluted FT-IR spectra of GO and graphene oxide crosslinked chitosan beads.

The FT-IR spectra of graphene oxide crosslinked Chitosan beads show a combination of characteristics similar to that of the pristine chitosan and graphene oxide which include the broad absorption band located at 3400 cm^{-1} assigned to the mixture of the amine stretch from the chitosan and to the OH groups in graphene oxide. The deconvoluted spectra show that the peak at 1620 cm^{-1} , which is assigned to the COOH groups of graphene oxide, is downshifted compared to pristine graphene oxide due to hydrogen bonding between the graphene oxide and hexatomic ring of the chitosan. The peak in the region about 1060 cm^{-1} is indicative of C–O–C stretching from the graphene oxide layers. The FT-IR results indicate the existence of a chemical interaction between chitosan and graphene oxide via hydrogen bonding.

X-ray diffraction of composite GOCH

Figure (14) presents XRD patterns of the pure graphite powder, GO and GOCH. Careful analysis of the figure reveals that the XRD pattern of the pure graphite exhibits a high intensity peak around 26.7°

corresponding to the graphitic structure (002). After the oxidation and exfoliation process, this peak disappears in the XRD pattern of the GO and a new peak is observed at $2\theta = 11.4^\circ$, corresponding to the (0 0 1) plane reflection of GO, which indicates that graphite was converted into GO. The calculated interlayer spacing of GO is 0.798 nm, which is much larger than that of graphite (0.336 nm). The larger interlayer distance of GO could be attributed to the oxide induced oxygen containing functional groups such as hydroxyl, epoxy and carboxyl. These assignments are in good agreement with those reported in literature [38-42].

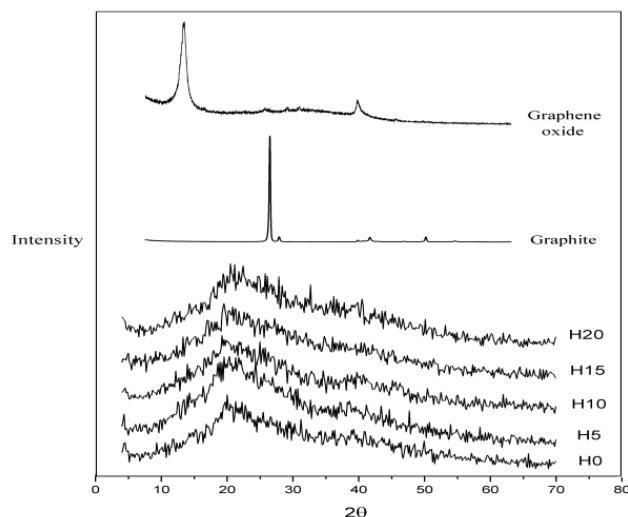


Figure 14: XRD pattern of graphite, graphene oxide and GOCH.

All of GOCH composites samples display a broad peak at $2\theta = 20.5^\circ$ due to the amorphous state of the chitosan and the diffraction peak of GO is not seen in the XRD patterns of GOCH composites. This indicates that the amorphous structure of chitosan dominated the GO and GO was well exfoliated with chitosan in GOCH composites. The XRD results therefore showed the good compatibility and mixability between GO and chitosan in the composites, because, if GO and Chitosan had low compatibility in the composite, each component would show its own Crystal region in the composite and the X-ray diffraction patterns should show a simply mixed pattern of GO and Chitosan. These results are in good agreement with the results reported by D Han et al [35].

Study of the factors affecting the efficiency of the Adsorption capacity of GO-Chitosan beads (GOCH):

Effect of pH value

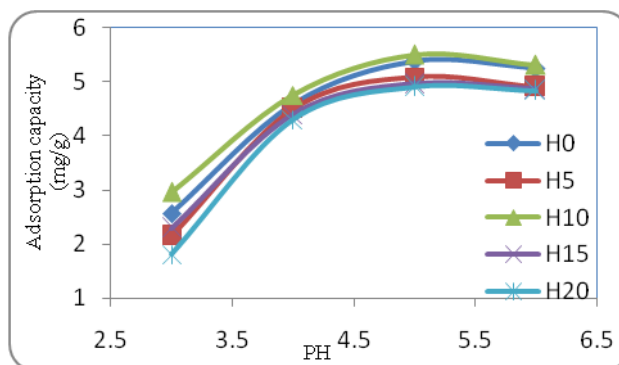


Figure 15: effect of pH value on the adsorption capacity GOCH.

As it shown in fig 15, the pH profile shows that the removal of Pb(II) ions increases as the solution pH increases and it reaches the maximum value at a pH of 5. An appreciable decrease in the adsorption capacity is observed after pH 5. At low pH values, the negative sites of the adsorbent was occupied by the H^+ and H_3O^+ ions which leads to a reduction of vacancies for Pb(II) ions and consequently causes a decrease in Pb(II) ions adsorption. As the solution pH was increased, the ability of Pb(II) ions for competition with protons was also increased. Although the adsorption of metal ions was found to be raised by increasing solution pH, further increment of pH caused declining in adsorption due to the formation of metal hydroxides. However, a pH value of 5.0 was chosen as optimum for further experiments to avoid the formation of metal hydroxides.

Influence of initial adsorbent doses

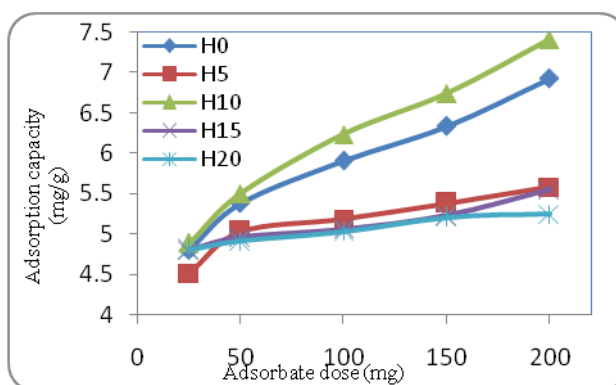


Figure 16: effect of the initial adsorbent dose in (mg) on

Adsorption capacity (mg/g_w) of GOCH

It can be seen from the figure (16) that the removal of Pb(II) ions increases with increasing GOCH dose due to the availability of more binding sites on the beads surface and reaches almost a constant value which may be due to the reduction in concentration gradient and also due to overlapping or aggregation of adsorption sites resulting in a decrease in total adsorbent surface area. Further adsorption equilibrium study will be conducted using 0.2 g beads for which the adsorption capacity was the highest.

Influence of contact time

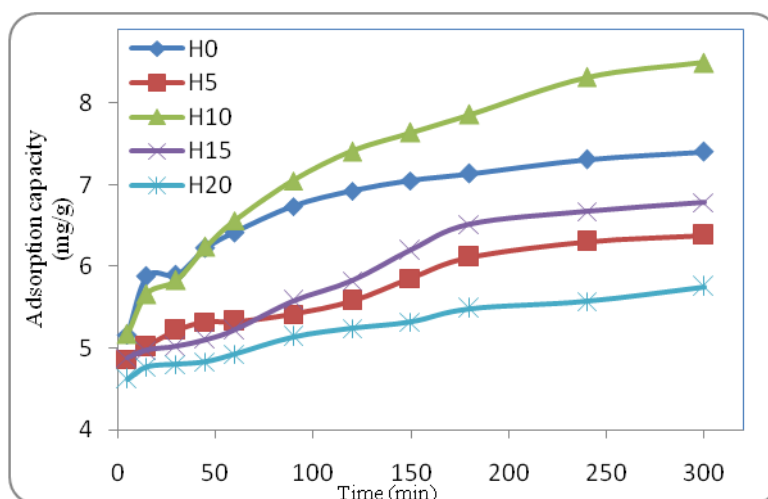


Figure 17: The relation between contact time and the adsorption capacity (mg/g_w) of GOCH.

Generally, as it shown in figure (17), the removal of Pb(II) ions is initially rapid, but it gradually decreases with time until equilibrium is reached. The removal of Pb(II) ions is higher at the beginning due to

the availability of more active sites for the adsorption of the lead(II) ions. As the active sites become exhausted, the rate of uptake of Pb(II) ions is controlled by the rate of transport of Pb(II) ions from the exterior to the interior sites of the adsorbent.

Also it can be seen from the figure that the adsorption capacity is influenced by the composites molar ratios, the maximum adsorption capacity was recorded for the samples H10 (removal percentage 90%). This means that concentration of 10% of the GO in the composite can enhancing the adsorption capacity of Pd(II) compared with the chitosan.

EDX Analysis

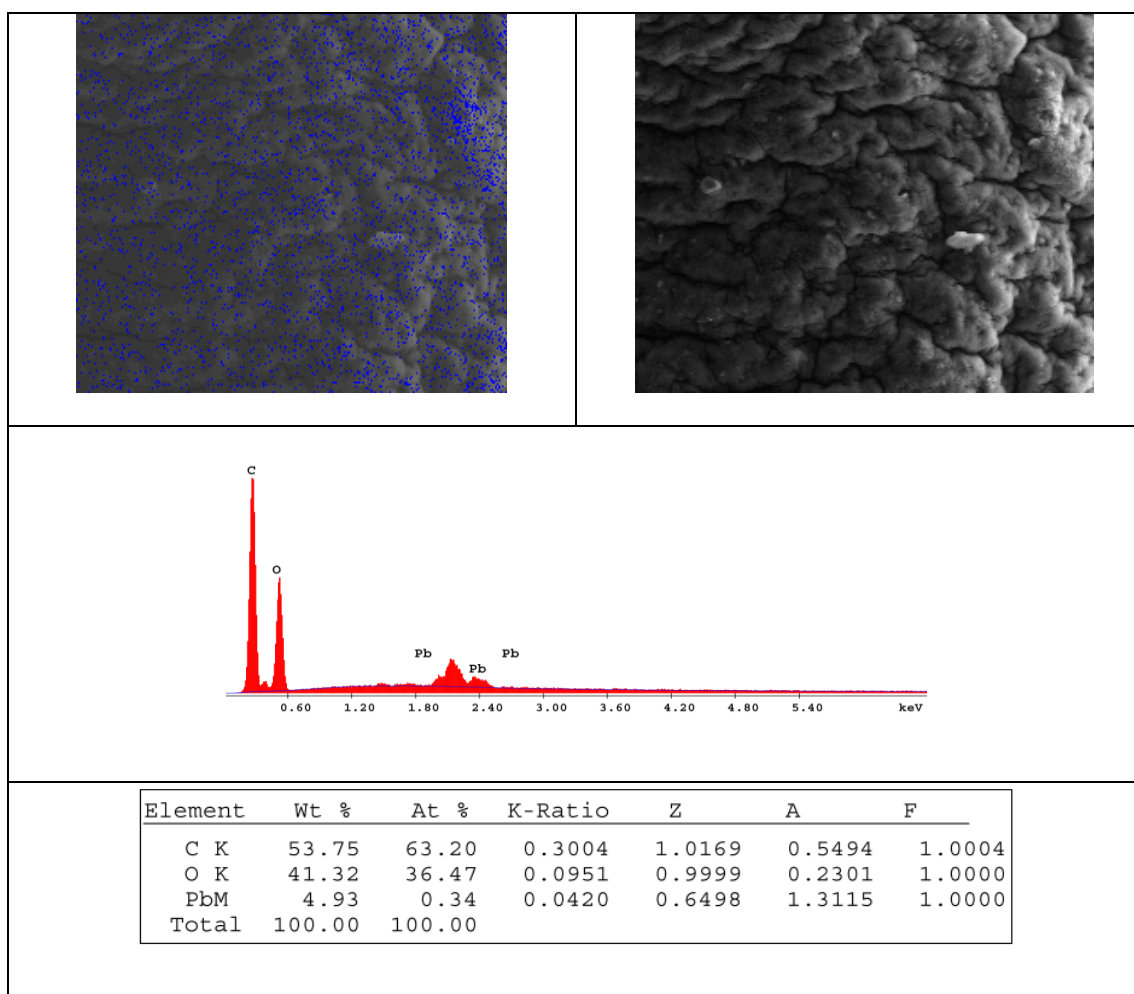


Figure 18: EDX analysis of GO chitosan composite (H10).

Figure 18 displays the EDX mapping for element distribution of GOCH sample H10 after Pb ions adsorption, which indicates the homogeneous distribution of (Pb) adsorbed on the polymer matrix and within the pores sites of the beads. It could be clearly seen that the Pb percentage in the sample showed homogeneous distribution and represented about 4.93 % from the total weight of the nanocomposite GOCH, sample H10.

Adsorption kinetic Mechanisms

The typical results from the kinetic adsorption study with the beads showed that high adsorption rates for lead ions (i.e., rapid change of concentrations with time) occurred in the initial stage of the adsorption process and the adsorption process finally reached the adsorption equilibrium in about 180min. Metal sorption kinetics are influenced by sorption reactions and the mass transfer steps that govern the

transfer of metal ions from the bulk of the solution to the sorption sites on the surface and inside adsorbent particles, i.e. external and intra-particle diffusion.

For this purpose, simplified models can be used to test experimental batch data and identify the rate-controlling mechanisms for the adsorption process. Of these models, the pseudo first-order model, the pseudo second-order model, and the intra-particle diffusion model are the most widely used to describe the sorption of metal ions. The goodness of the fit was estimated in terms of the coefficient of determination, R^2 and compatibility between the calculated equilibrium adsorption capacities q_e with the experimental values.

Pseudo-First-Order kinetic model

The Lagergren rate equation was the first rate equation for sorption in a liquid/solid system based on solid capacity. This equation can be linearized for use in the kinetic analysis of experimental results. The linear pseudo-first order kinetic model of Lagergren is given as [43]:

$$\text{Log}(q_e - q_t) = \text{Log} q_e - \frac{K_1}{2.303} t \quad (3)$$

Where q_e and q_t are the amounts of Pb(II) ions adsorbed onto beads (mg/g) at equilibrium and at time t , respectively, and k_1 is the rate constant of pseudo-first order kinetic model (min^{-1}). The straight-line plots of $\log(q_e - q_t)$ against t were used to determine the k_1 and correlation coefficient, R^2 . Table (1) shows the calculated values of K_1 , q_e (theo.), q_{exp} (experimental) and R^2 (correlation factor).

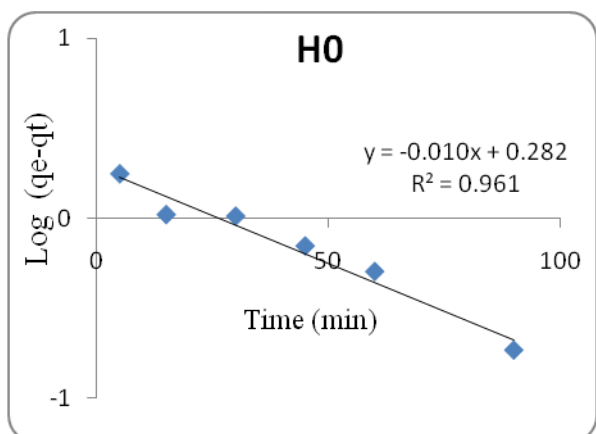


Figure 19: the relation between time t (min) and $\text{Log}(q_e - q_t)$ for crosslinked chitosan (H0)

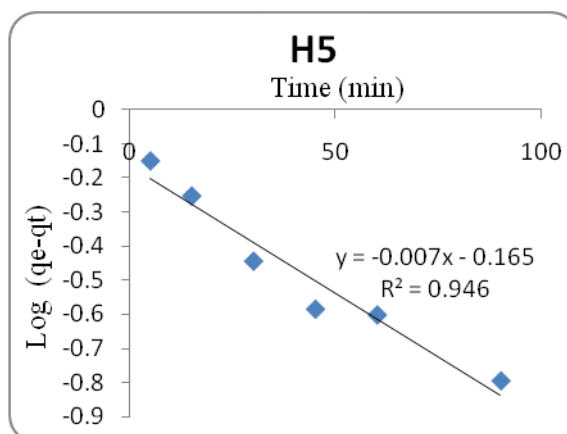


Figure 20: the relation between time t (min) and $\text{Log}(q_e - q_t)$ for crosslinked GO/chitosan (H5)

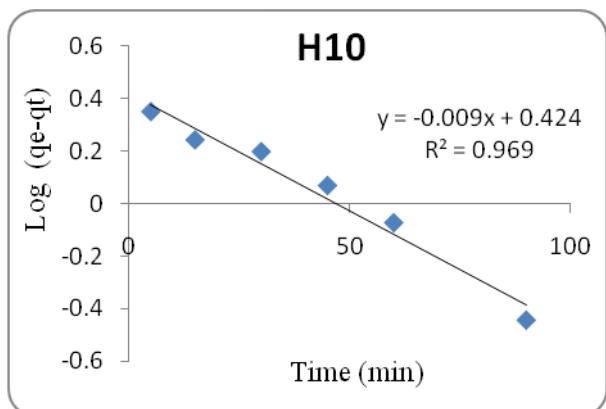


Figure 21: the relation between time t (min) and $\text{Log}(q_e - q_t)$ for crosslinked GO/chitosan (H10)

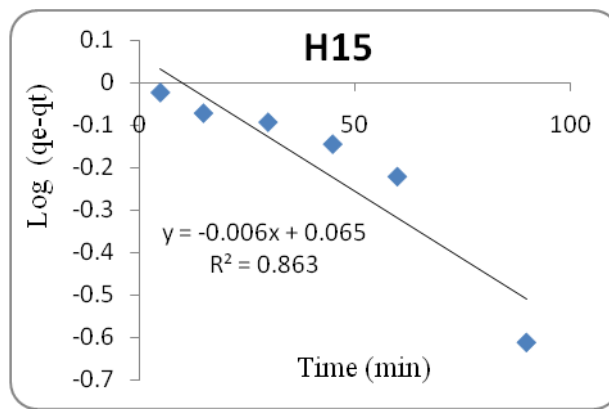


Figure 22: the relation between time t (min) and $\text{Log}(q_e - q_t)$ for crosslinked GO/chitosan (H15)

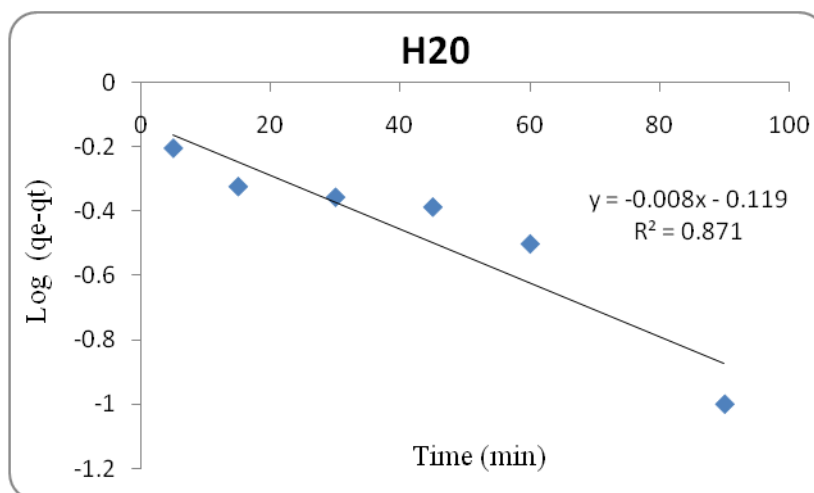


Figure 23: the relation between time t (min) and Log(qe-qt) for crosslinked GO/chitosan (H20)

Table 1: The calculated values of K1, qe (theo.), qexp (experimental) and R²(correlation factor).

Pseudo first-order kinetic model: $\log (q_e - q_t) = \log q_e - k_1 \cdot t/2.303$				
	K1	Qe	qexp	R ²
H0	0.0230	1.914	7.14	0.961
H5	0.0161	1.462	6.115	0.946
H10	0.0207	2.654	7.865	0.969
H15	0.0138	1.161	6.52	0.863
H20	0.0184	1.315	5.49	0.871

Pseudo-second order kinetic model:

The linear form of the pseudo-second-order equation is given by:

$$\frac{t}{qt} = \frac{1}{K_2 qe^2} + \frac{1}{qe} T \quad (4)$$

Where qe and qt are the amounts of Pb(II) ions adsorbed onto beads (mg/g) at equilibrium and at time t, and k2 is the rate constant of pseudo-second order kinetic model (g/mg.min). The straight-line plots of t/qt against t were used to determine the correlation coefficient, R². The pseudo-second order kinetic model was used to determine whether the rate limiting step during the adsorption process was chemisorption. This model was more likely to predict the behavior over whole range of contact time. Table (2) shows pseudo-second order kinetic model calculated values of K2, qe (theo.), qexp (experimental) and R² (correlation factor).

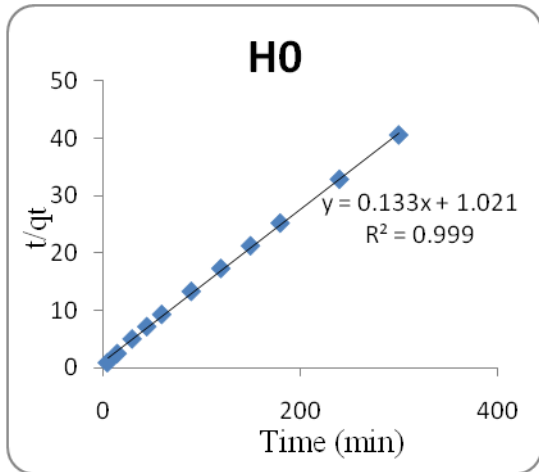


Figure 24: the relation between t/qt versus time t (min) for crosslinked chitosan (AH0)

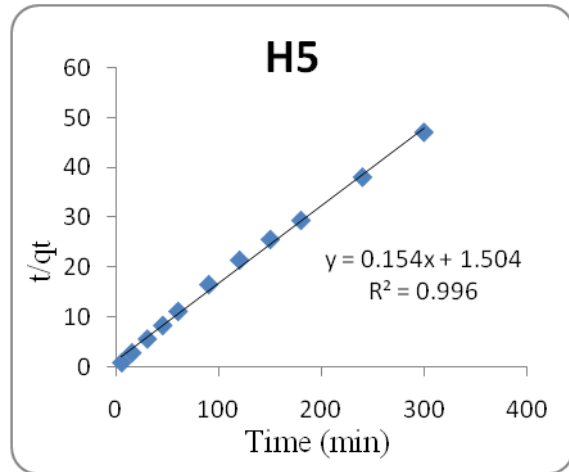


Figure 25: the relation between t/qt versus time t (min) for crosslinked GO/chitosan composite (H5)

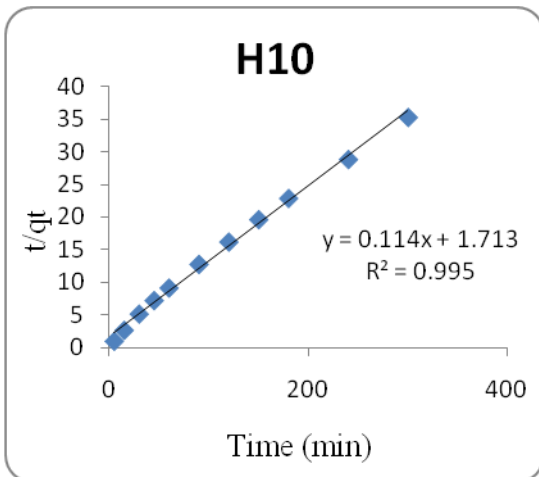


Figure 26: the relation between t/qt versus time t (min) for crosslinked GO/chitosan composite (H10)

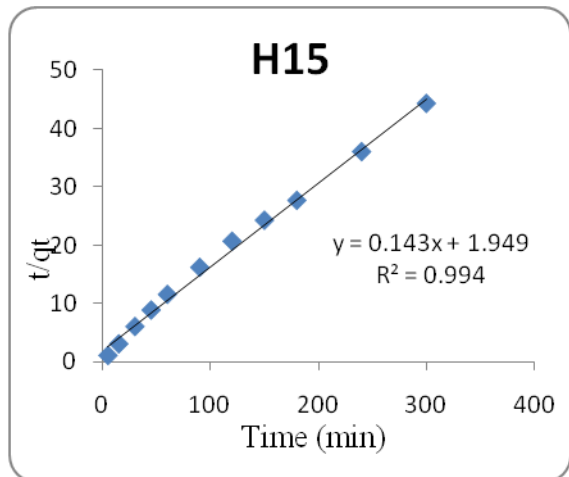


Figure 27: the relation between t/qt versus time t (min) for crosslinked GO/chitosan composite (H15)

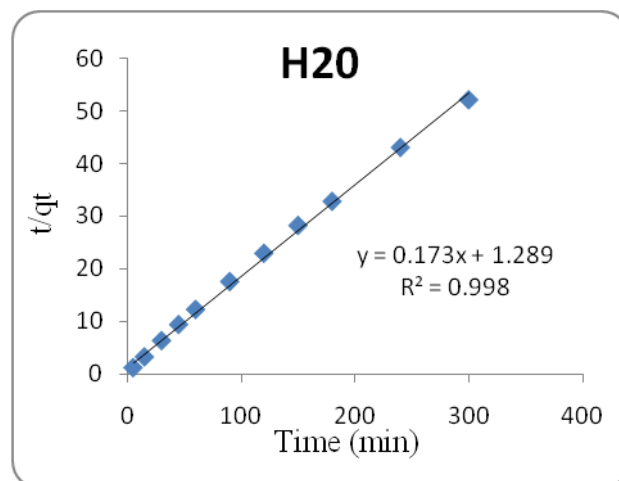


Figure 28: the relation between t/qt versus time t (min) for crosslinked GO/chitosan composite (H20)

Table 2: The calculated values of K2, qe (theo.), qexp (experimental) and R² (correlation factor).

Pseudo second-order kinetic model: $t/q_t = 1/k_2 \cdot q_e^2 + 1/q_e \cdot T$				
	K2	qe	qexp	R ²
H0	0.1303	7.512	7.14	0.999
H5	0.1029	6.46	6.115	0.996
H10	0.0671	8.703	7.865	0.996
H15	0.0738	6.954	6.52	0.995
H20	0.135	5.764	5.49	0.998

Interparticle diffusion model

The adsorbate can be transferred from the solution phase to the surface of the adsorbent in several steps. The steps may include film or external diffusion, pore diffusion, surface diffusion and adsorption on the pore surface. The overall adsorption can occur through one or more steps. To investigate the internal diffusion mechanism during the adsorption of metal ions onto beads, the intra-particle diffusion equation has been used.

Intraparticle diffusion is characterized by the relationship between specific sorption (qt) and the square root of time according to Equation (5).

$$qt = K_{Int} * t^{1/2} \dots\dots (5)$$

Where qt is the amount of Pb ions adsorbed onto adsorbent material (mg/g) at time t , and k_{int} is the intraparticle diffusion rate constant (mg/g min^{1/2}). According to Weber and Morris [44], if the intra-particle diffusion is the rate-limiting step in the adsorption process, the graph of qt vs. $t^{0.5}$ should yield a straight line passing through the origin. McKay and Allen [45] suggested three linear sections on the plot qt vs. $t^{0.5}$ can be identified. That means that two or three steps can occur

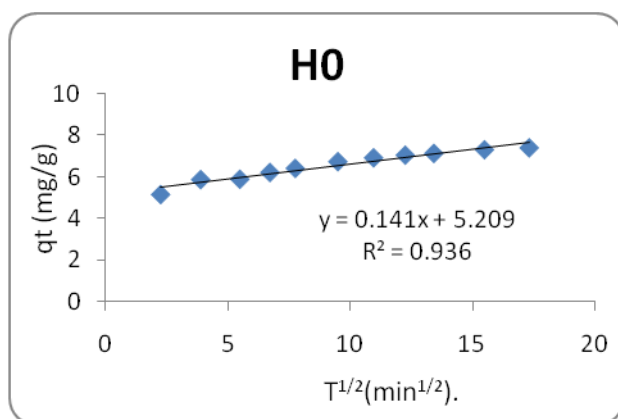


Figure 29: the relation between qt (mg/g) versus square root of contact time $t^{1/2}$ (min^{1/2}) of crosslinked chitosan (H0)

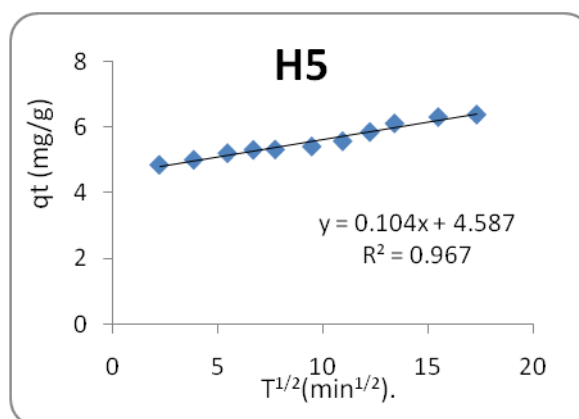


Figure 30: the relation between qt (mg/g) versus square root of contact time $t^{1/2}$ (min^{1/2}) of crosslinked GO/chitosan (H5)

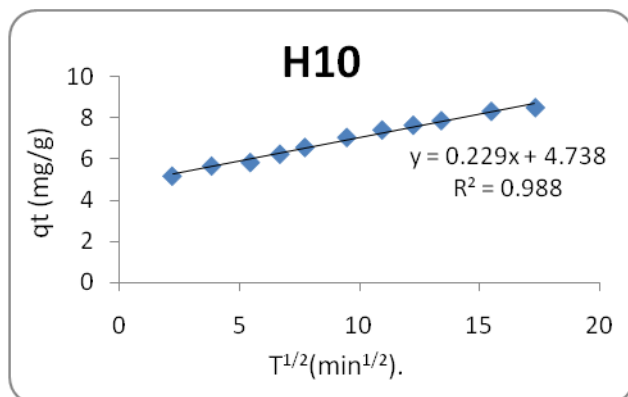


Figure 31: the relation between q_t (mg/g) versus square root of contact time $t^{1/2}$ ($\text{min}^{1/2}$) of crosslinked GO/chitosan (H10)

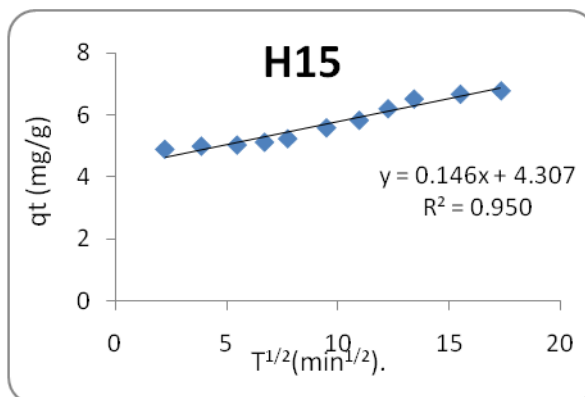


Figure 32: the relation between q_t (mg/g) versus square root of contact time $t^{1/2}$ ($\text{min}^{1/2}$) of crosslinked GO/chitosan (H15)

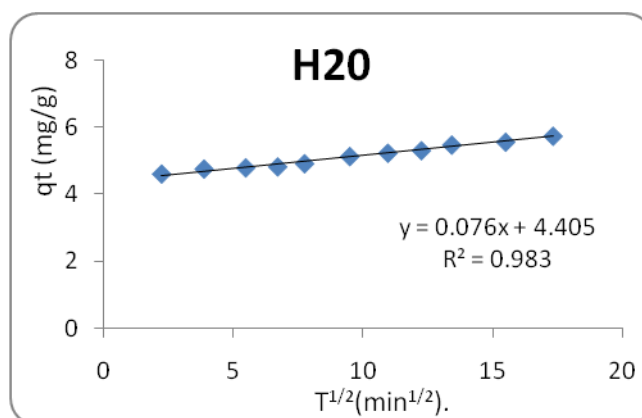


Figure 33: the relation between q_t (mg/g) versus square root of contact time $t^{1/2}$ ($\text{min}^{1/2}$) of crosslinked GO/chitosan (H20)

The results reveal that Pb(II) adsorption by the chitosan and the GO crosslinked chitosan beads best can be described by pseudo-second-order equation (R^2 values ~ 0.996 and was very high and close to unit). The calculated equilibrium adsorption capacities q_e were very compatible with the experimental values. Therefore, the Pseudo-second-order kinetic model is predominant for GOCH and the rate-limiting step was chemisorption. The intraparticle diffusion was not the only rate-controlling step and the adsorption of Pd(II) onto GOCH was a complex process [44,45].

CONCLUSION

Due to its large specific surface area, abundant functional groups, good dispersibility in water, relatively easy preparation methods and better biocompatibility, GO demonstrates the possibility of applying it as an excellent waste water treatment agent. From the view of environment and economy, biopolymers attract a strong interest as a more environmental and cost effective alternative. From the obtained data it was concluded that the obtained GO appeared as individual nanosheets and these nanosheets have sizes extending from tens to several hundreds of square nanometers. Also it was concluded that the addition of GO to chitosan increases folding, and roughness of composites surface that in turn lead to an increase the surface area and consequently enhancing the adsorption capacities of the composites. The GO showed well exfoliated within chitosan matrix. These applicable crosslinked beads with high porosity and spherical forms are easily swellable in water and demonstrated as a good adsorbent due to its high surface area.

The infra red spectra showed that crosslinking of chitosan with Na-tripolyphosphate (TPP) resulted in the appearance of a new peak at 1253 cm^{-1} which corresponds to the attachment of TPP molecule to the

nitrogen atom in chitosan. In addition FT-IR spectra of GOCH composites with different molar ratios showed that there is a chemical interaction between GO and the chitosan chains via hydrogen bonding.

The XRD pattern of graphite and GO revealed that the original graphite powders had almost been completely oxidized and GO has been exfoliated successfully also the XRD results reflected the good compatibility and mixability between GO and the chitosan.

The factors affecting the adsorption capacity of the prepared composites such as pH value, initial adsorbent dose and contact time were investigated. The experimentally obtained results showed that the adsorption capacity depends strongly on pH and the optimum pH value is 5. While the optimum initial dose of adsorbent material is 0.2 gram. The sorption experiment study showed that GO can obviously enhance the adsorption property of chitosan, graphene oxide 10 wt% with chitosan composite had the largest adsorption removal for Pd(II) compared with the other prepared GOCH composites. The maximum adsorption removals were 90% for GOCH (H10) after 240 minutes.

Faster adsorption rates are always desirable in all adsorption separation processes. The typical results from the kinetic adsorption study with the beads showed that high adsorption rates for lead ions (i.e., rapid change of concentrations with time) occurred in the initial stage of the adsorption process and the adsorption process finally reached the adsorption equilibrium in about 180min.

Metal sorption kinetics are influenced by sorption reactions and the mass transfer steps that govern the transfer of metal ions from the bulk of the solution to the sorption sites on the surface and inside adsorbent particles, i.e. external and intra-particle diffusion. In turn, these mechanisms depend on the physical form of the adsorbents, the intrinsic structure, the nature of the metal and the solution, as well as, process conditions (temperature and pH).

For this purpose, Simplified models can be used to test experimental batch data and identify the rate-controlling mechanisms for the adsorption process. Of these models, the pseudo first-order model, the pseudo second-order model, and the intra-particle diffusion model are the most widely used to describe the sorption of metal ions. The goodness of the fit was estimated in terms of the coefficient of determination, R^2 and compatibility between the calculated equilibrium adsorption capacities q_e with the experimental values.

The Pseudo-second-order kinetic model is predominant for GOCH and the rate-limiting step was chemisorption. The intraparticle diffusion was not the only rate-controlling step and the adsorption of Pd(II) onto GOCH was a complex process.

The applicable form of GO-nanocomposites beads prepared as spherical carriers with high porosity structure is easily swellable in water and demonstrates a great potential in the efficient removal of lead ions from wastewater. In addition, from the view of environment and economy, biosorbents attract a strong interest as a more environmental and cost effective alternative, this method of preparation is simple, economical and environmental friendly.

REFERENCES

- [1] <http://www.cheresources.com/biosorption.shtml>.
- [2] K Jüttner, U Galla, and H Schmieder. *Electrochimica Acta*, 45 (2000), 2575–2594.
- [3] X.J. Yang, A.G. Fane and S. Mac Naughton, *Water Science and Technology*, 43 (2001), 341–348.
- [4] P. Bose, M.A. Bose, and S. Kumar, *Advances in Environmental Research*, 7 (2002), 179–195.
- [5] U. Wingenfelder, C. Hansen, G. Furrer, and R. Schulin, *Science and Technology*, 39 (2005), 4606–4613.
- [6] N.K. Shammass, "Coagulation and flocculation" in *Physicochemical Treatment Processes*, edited by L.K. Wang, Y.T. Hung and N.K. Shammass, Humana Press, New Jersey, (2004).
- [7] L. Semerjian, and G.M. Ayoub, *Advanced Environmental Research*, 7 (2003), 389–403.
- [8] Licskó, *Water Science and Technology*, 36 (1997), 103–110.
- [9] G.M. Ayoub, L. Semerjian, A. Acra, M. El Fadel, and B. Koopman, *Journal of Environmental Engineering*, 127 (2001), 196–202.
- [10] Metcalf and Eddy, *Wastewater Engineering: Treatment and Reuse*. McGraw Hill International Edition, New York (2003).

- [11] W. W. Eckenfelder, *Industrial Water Pollution Control*, McGraw-Hill Companies, (2000).
- [12] F. Rouquerol, *Adsorption by Powders and Porous Solids*, Academic Press, London, (1999).
- [13] N.C. Sawyer, P.L. Mc Carty, G.F. Parkin, *Chemistry for Environmental Engineering*, Mc. Graw Hill International Edition, Singapore, (1994).
- [14] J.M. Montgomery, *Water Treatment Principles and Design*, Consulting Engineers Inc. USA, (1985).
- [15] P.V. Atkins, *Physical Chemistry*, Oxford University Press, 5th Edition, Oxford, (1994).
- [16] Jiang HJ. *Small*. 2011; 7(17): 2413-2427.
- [17] Guo SJ, Dong SJ. *Chem Soc Rev*. 2011; 40(5): 2644-2672.
- [18] Willi Paul and Chandra P. Sharma, *Trends Biomater. Artif. Organs*, 25(3), 91-94 (2011).
- [19] C.M. Hasfalina, R.Z. Maryam, C.A. Luqman, M. Rashid, *J. Nat. Fibers* 7 (2010) 267.
- [20] E. Guibal, *Sep. Purif. Technol.* 38 (2004) 43.
- [21] M.L.P. Dalida, A.F.V. Mariano, C.M. Futralan, C.C. Kan, W.C. Tsai, M.W. Wan, *Desalination* 275 (2011) 154.
- [22] M.M. Lou, B. Zhu, I. Muhammad, B. Li, G.L. Xie, Y.L. Wang, H.Y. Li, G.C. Sun, *Carbohydr. Res.* 346 (2011) 1294.
- [23] R.R. Araiza, P. Alcouffe, C. Rochas, A. Montebault, L. David, *Langmuir* 26 (2010), 17495.
- [24] H. Sashiwa, S. Aiba, *Prog. Polym. Sci.* 29 (2004) 887.
- [25] S.H. Lim, S.M. Hudson, *Color Technol.* 120 (2004).
- [26] W.S. Wan Ngah and S. Fatinathan, *Journal of Environmental Management*, 91 (2010) 958–969.
- [27] W Bin, C Yan-hong, ZHI Lin-jie. *New Carbon Materials*, (2011), 26(1):31–35.
- [28] Qiu Huamin, Fan Lulua, Xiangjun Li, Leilei Li a, Sun Mina,b, Luo Chuannan. *Carbohydrate Polymers* 92 (2013) 394– 399
- [29] T Chen¹, Baoqing Zeng, J L Liu, J H Dong , X Q Liu, Z Wu¹, X Z Yang and Z M Li. *Journal of Physics: Conference Series* 188 (2009).
- [30] Xiangang Hua, Li Mub, Jianping Wenb, Qixing Zhou. *Journal of Hazardous Materials* 213– 214 (2012) 387– 392
- [31] Fan HL, Wang LL, Zhao KK. *Biomacromolecules*. (2010); 11(9): 2345-2351.
- [32] Hummers, W. S., & Offeman, R. E.. *Journal of the American Chemical Society*, (1958) 80(6), 1339.
- [33] Karthikeyan Krishnamoorthy, Murugan Veerapandian, Kyusik Yun b, S.-J. Kim. *CA R B O N*, 5 3 (2013) 3 8 –4 9
- [34] Guoxiu Wang, Bei Wang, Jinsoo Park, Juan Yang, Xiaoping Shen, Jane Yao. *C A R B O N* 4 7 (2009) 6 8 –7 2.
- [35] Donglin Han, Lifeng Yan, Wufeng Chen, Wan Li. *Carbohydrate Polymers* 83 (2011) 653–658
- [36] M. R. de Moura, F. A. Aquada, L. HC. Mattoso, *Journal of colloid and interface science*, 321 (2008), 477-483.
- [37] P. Monvisade and P. Siriphannon, *Applied Clay Science*, 42 (2009), 427-431.
- [38] V.S. Channua, R. Bobbab, R. Holze. *Colloids and Surfaces A: Physicochem. Eng. Aspects* 436 (2013) 245–251.
- [39] Tapas Kuilla , Sambhu Bhadra, Dahu Yaaa, Nam Hoon Kimc, Saswata Bosed, Joong Hee Leea,d. *Progress in Polymer Science* 35 (2010) 1350–1375.
- [40] Ashish Kumar Mishra, S. Ramaprabhu. *Desalination* 282 (2011) 39–45.
- [41] Son Truong Nguyena, Hoa Tien Nguyenb, Ali Rinaldic, Nam P.V. Nguyena, Zeng Fana, Hai Minh Duonga. *Colloids and Surfaces A: Physicochem. Eng. Aspects* 414 (2012) 352– 358
- [42] Jin-Yeon Kong a, Myeon-Cheon Choi a, Gwang Yeon Kim a, Jin Joo Park a, M. Selvaraj b, Mijeong Han c, Chang-Sik Ha. *European Polymer Journal* 48 (2012) 1394–1405
- [43] Y.S.Ho and G.McKay, *Trans. Inst. Chem. Eng.* 76B (1998), 332–340.
- [44] W.J. Weber and J.C. Morris, *Water Research*, 89 (1963), 31–59.
- [45] McKay, G. and S. J. Allen. *Can. J. Chem. Eng.* (1980) 58, pp. 521.
- [46] Nabila S. Ammar, Hanan Elhaes, Hanan S. Ibrahim, Walid El hotaby, Medhat A. Ibrahim (2014) A novel structure for removal of pollutants from wastewater. *Spectrochimica Acta Part A: Molecular and Biomolecular Spectroscopy*, 121: 216-223.
- [47] M.A. moharram, F.M. Reicha, N. Kinawy and Walid El Hotaby, (2012) Factors Controlling The Adsorption Capacity Of Crosslinked Chitosan Beads And Natural Montmorillonite Powder: Comparative Study. *Journal of Applied Sciences Research*, 8(11): 5425-5435